

Lab on a Chip

Accepted Manuscript



This is an *Accepted Manuscript*, which has been through the Royal Society of Chemistry peer review process and has been accepted for publication.

Accepted Manuscripts are published online shortly after acceptance, before technical editing, formatting and proof reading. Using this free service, authors can make their results available to the community, in citable form, before we publish the edited article. We will replace this *Accepted Manuscript* with the edited and formatted *Advance Article* as soon as it is available.

You can find more information about *Accepted Manuscripts* in the [Information for Authors](#).

Please note that technical editing may introduce minor changes to the text and/or graphics, which may alter content. The journal's standard [Terms & Conditions](#) and the [Ethical guidelines](#) still apply. In no event shall the Royal Society of Chemistry be held responsible for any errors or omissions in this *Accepted Manuscript* or any consequences arising from the use of any information it contains.

ARTICLE

Cite this: DOI: 10.1039/x0xx00000x

Received 00th January 2012,
Accepted 00th January 2012

DOI: 10.1039/x0xx00000x

www.rsc.org/

Versatile multiple protein nanopatterning within a microfluidic channel for cell recruitment studies

A.S. Andersen^a, W.F. Zheng^b, D. S. Sutherland^a and X.Y. Jiang^b

A novel approach combining self-assembly based colloidal lithography and Polydimethylsiloxane (PDMS) micro-molding to generate complex protein nanopatterns for studying mechanisms of leukocyte extravasation within microchannels is presented. Nanostructured surfaces sealed onto PDMS molded microchannels are chemically functionalized in-situ in an all aqueous process to generate bi-functional chemical nanopatterns. Subsequent co-immobilization with proteins makes use of common non-covalent coupling (e.g. HIS-tags, FC-tags and biotin-tags) giving nanopatterns of arbitrary combinations of oriented, functional proteins. Up to three different proteins were simultaneously co-immobilized into the microchannel with nanoscale precision demonstrating complex patterns. As proof-of-principle a mimic of inflamed endothelium was constructed using a macro and nanoscale pattern of intercellular adhesion molecule 1 (ICAM1) and P-selectin, and measuring the response of leukocytes through live cell imaging. A clear result on the rolling behavior of the cells was observed with rolling limited to areas where ICAM1 and P-selectin is present. This micro/nano-interface will open new doors to investigations of how the spatial distributions of proteins control cellular activity.

Introduction:

Leukocyte recruitment to a site of infection is a complex and crucial part of the immune system. It is a multistep process generally divided into four parts, namely rolling adhesion, tight binding, diapedesis and migration.¹ In vivo studies are complicated by the large number of interactions involved which necessitates in vitro experiments to gain a detailed understanding each molecule and its role in the overall picture. A great volume of studies have been performed and today we have a good understanding of some processes involved.²⁻⁷ Still there are many unknowns especially on how different ligands interact together with each other and how the micro- and nano-scale distributions of these ligands influence the cell behavior. Thus there is a need for in vitro systems that allow the study of cells interacting with multiple ligands distributed with both micro- and nano-scale precision. To study the initial step in leukocyte recruitment it is essential to have a flow condition mimicking blood flow and to be able to analyze the results in real time. Microfluidics allows the study of flow systems especially blood flow because the geometry of the channels can precisely mimic that of blood vessels.⁸ Microfluidic systems also have the advantage of requiring very low amounts of liquids and solutes, making it a cost-effective way of patterning proteins. It has been used to investigate complex processes⁹⁻¹¹ and can mimic various flow related mechanisms in vitro¹²⁻¹⁴. Since the components of microfluidic systems are relatively small, the whole setup can be conveniently incorporated onto a fluorescence microscope to allow real-time imaging of live cells inside the channel.^{9, 15-17} By incorporating protein patterns into microchannels, a new set of tools for further manipulation of the pattern are available.¹⁸ Even though it offers great potential, there have been relatively few examples of protein patterns within microchannels^{11, 19, 20} and, to the best of our knowledge, no build-in-channel nanopatterns of proteins has been reported. Micro and nanostructured surfaces have been widely applied as tools to mimic the complexity of the in vivo cellular microenvironment and clearly shown that patterns and structures have strong modulation on cellular adhesion, proliferation and differentiation.²¹⁻²³ An early landmark study used micropatterns of fibronectin to show a correlation between cell spread area and survival,²⁴ later studies established cell shape and associated cytoskeletal organization as a critical parameter in cell differentiation.²⁵ Nanostructured materials have been used to correlate the organization of cell ligands at the nanoscale to cell adhesion and adhesive complex development²⁶⁻³⁰ as well as signal transduction and downstream differentiation³¹⁻³⁴ in efforts both to study mechanisms and control cells for tissue engineering applications. Detailed cellular responses to their environment were studied by the use of sub-cellular and molecular level patterning.^{29, 30, 35-37} Subcellular protein and cell-ligand patterns for studying the behavior and function of adherent cells are typically in the form of single-type protein patterns (lateral distributions of a single protein type) and applied in static culture conditions. Despite the simplification of the cellular microenvironments of the single-type protein patterns, such approaches have been central in advancing the understanding of cellular microenvironments.^{26, 27, 38-40} There is a clear need however for increasing the complexity of the cellular microenvironments including both multiple co-patterned cell ligands and allowing the study of cell adhesion dynamically.³⁹ In particular for understanding adhesion of cells circulating in the bloodstream, e.g. leukocytes, it is vital to include both the components of flow and multi-ligand adhesion mechanisms which are critically present in vivo. One of the important ligands for leukocytes is ICAM1 (intercellular adhesion molecule 1), which is critical for a tight binding to the endothelial surface.⁴¹ Selectins are a special type of ligands that are needed for the initial rolling of the cells, three have been identified being P, E and L selectin, where P and E are found on endothelial cells.⁴² Recent directions in cancer therapy are addressing the importance of both immune cell evasion and cancer cell arrest at the endothelium allowing extravasation and remote tumor formation.⁴³ Here we overcome critical technical challenges to demonstrate a method to prepare co-localized protein

nanopatterns within microfluidic channels. We have developed a colloidal nanopatterned template which can seal to a PDMS (Polydimethylsiloxane) microchip and an all aqueous chemical functionalization to allow subsequent in situ assembly of protein nanopatterns. We demonstrate both antibody arrays and co-localization of a dual nanopattern within a 3-way micropattern of 3 separate cell binding ligands (ICAM1, P-selectin and E-selectin) mimicking the inflammation activated endothelium. The protein nanopattern shows high spatial control and reversibility of protein attachment both in the microscale and nanoscale regime. We further studied dynamic leukocyte-protein nanopattern interaction in a proof of principle experiment mimicking the initial two steps of cellular adhesion for the complex leukocyte recruitment in the microchannel. This multi-protein nanopattern system is promising in leukocyte recruitment and circulating tumor cell extravasation research.

Materials and methods:

Proteins and buffers:

The following molecules and proteins have been used in this study. Cysteamine, Streptavidin, Protein-A, BSA were from Sigma-Aldrich (www.sigmaaldrich.com). PLL-g-PEG and PLL-g-PEG NTA were from SuSoS (www.susos.com), ICAM-FC, Aequorea victoria GFP HIStagged, P-selectin HIStagged, and E-selectin HIStagged were from Sinobiological (www.sinobiological.com), Anti-Paxilin rabbit antibody was from Santa Cruz biotechnology (www.scbt.com). Anti-rabbit Donkey TRITC antibody was from Jackson ImmunoResearch (www.jreurope.com). Buffers used are TRIS buffer: 100 mM TRIS adjusted to pH 9, HEPES buffer: 10 mM HEPES adjusted to pH 7.4 and Ringers buffer: 10mM HEPES, 7.2 mM KCL and 154 mM NaCl adjusted to pH 7.4.

Microfluidic device fabrication:

Rectangular glass slides (Menzel-gläser) were cleaned with N₂(g) and plasma (50W, reactive ion etcher - Advanced Vacuum) before having a 2 nm Ti layer and 10nm Au layer deposited via E-beam deposition (Cryofox – Polytechnik). Before any further use the samples were cleaned with 1h UV/ozone and 1h in a MQ water bath. Colloidal lithography was performed directly on the Au surface, by sequentially adding three layers of charged polymer in a liquid solution, with a N₂(g) drying step in between. The polymers added were 2 wt% PDDA (polydiallyldimethylammonium, Sigma-Aldrich), 2 wt% PSS (polysodium 4-styrene-sulfonate, Sigma-Aldrich) and 5 wt% PAX-XL60 (polyaluminium chloride, Kemira Miljø). The resulting positively charged Au surface was then incubated over night with an 8% w/v solution of sulphate-latex particles (Invitrogen), particle diameters used were 800 nm, 500 nm, 300 nm and 200 nm. After rinsing, The samples were heated to 120 °C in pressure chambers and dried with N₂(g). A new layer of 2 nm Ti and 10 nm SiO₂ were deposited by E-beam deposition on the colloidal patterned sample, and by tape stripping and sonication the particles were removed. This protocol completes the nanopatterned substrate.

To generate the microfluidic channel-embedded top piece, PDMS (Polydimethylsiloxane, Sylgard® 184 silicone elastomer kit, Dow Corning) was mixed in a 10:1 base-to-curing agent ratio, degassed, added to the silica wafer master (that has the microfluidic channel structures), degassed again and left to cure at 60 °C for 1h. The PDMS slab with channels was peeled off the master and was cut into appropriate sizes, before making holes for inlets and outlet. PDMS slab and the nanopattern were irreversibly bonded by plasma treatment (15W, reactive ion etcher, Advanced Vacuum). Inlet and outlet tubes were attached and deionized water was added to the channels, until the biofunctionalization step, to keep the PDMS hydrophilic inside the channel.

Biofunctionalization:

All functionalization was done by injecting liquids into the channel with 1 mL syringes. Channels were incubated with ~100 µL 2 mM cysteamine in Tris buffer for 30 min, washed with Tris then with HEPES. 0.25 mg/mL PLL-g-PEG mixed with 0.25 mg/mL PLL-g-PEG NTA (80% / 20% respectively) in HEPES was filtered through a 200 µm filter and incubated for 1 h in the channel, before being washed with first HEPES, then Ringer's solution. Sequential incubation of 100 µg/mL streptavidin in Ringers for 2 h, 2 wt% BSA in Ringers for 30 min and 20 µg/mL protein-A in Ringers for 1 h were then performed with washing steps in between. In all cases ~100 µL was injected. Depending on the sample type different routes were used from this stage. Either a primary (1:100) and secondary (1:100) antibody or labeled ICAM1-FC (5 µg/mL) was attached to protein-A. To attach proteins to the NTA groups they were activated by adding 5 mM NiCl₂ for 5 min. Three different HIS-tagged proteins were used: GFP (green fluorescent protein), P-selectin labelled with AF647 and E-selectin labelled with AF555, all added in a concentration of 42 nM in Ringers buffer. Figure 1 shows a schematic illustration

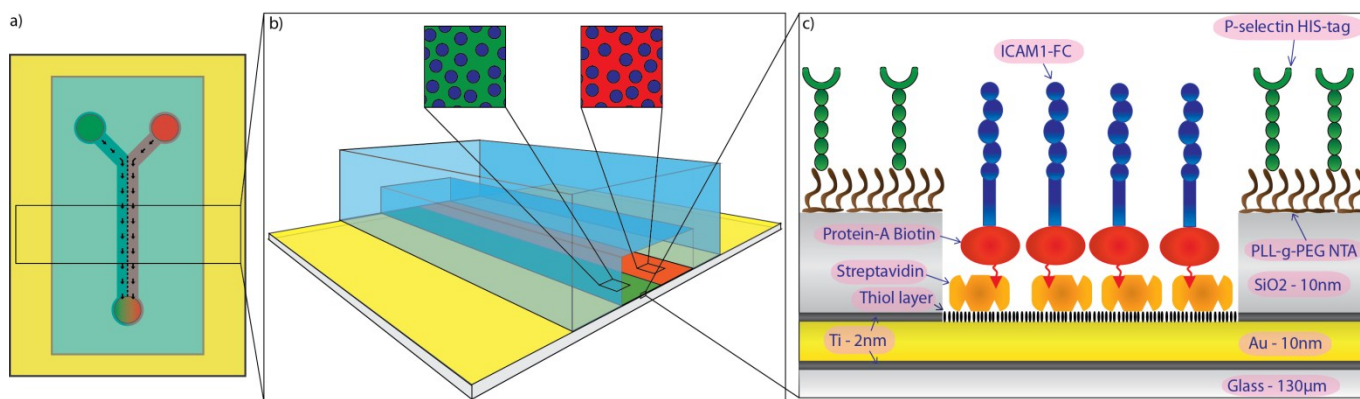


Figure 1: Schematic illustration of a multi-protein nanopattern inside a Y-shaped microchannel. a) A Y-shaped microchannel is used to form two laminar flows, parallel to each other, enabling site-specific adsorption of different proteins. b) Schematic overview of the microfluidic system. A PDMS slab containing a Y-shaped microchannel is bonded onto the surface of a piece of glass coverslide covered with Au nanopatterns and surrounding SiO₂. Two parallel streams of laminar flow could be formed in the microchannel and modify the corresponding regions with different proteins. c) The cross section of a single Au nanopattern and surrounding SiO₂ region is shown. On the surface of the Au nanopattern (Hole), Thiol, streptavidin, Protein-A biotin, and FC-tagged ICAM1 were immobilized in sequence. On the surface of the SiO₂ region, PLL-g-PEG NTA and His-tagged selectin were immobilized in sequence. The PDMS and nanopattern is sitting on a thin glass coverslide, making the entire device transparent, allowing live imaging inside the channel and the thickness of the glass (130 μm) makes it possible to image the nanopatterned surface with the highest magnification optical lenses, directly in the channel.

of a biofunctionalized microfluidic device and distribution of proteins in the nanopattern. In some cases the proteins were added under flow. A pump (Model 200 Series, kdScientific) was used to control two 1mL syringes containing buffer with or without protein. These syringes were connected to the two inlets of the microchannel. The flow time varied from 30 min to 1 h depending on the protein used, and a flow rate of 400 μL/h were used.

Protein labeling:

Proteins were labelled with protein labelling kits from lifetechnologies following the instructions given. Kits used were: Alexa fluor 647 protein labelling kit (A20173) for P-selectin, Alexa fluor 555 protein labelling kit (A20174) for E-selectin and Alexa fluor 488 Antibody labelling kit (A20181) for ICAM1. Protein concentration and degree of labelling were measured on a Nanodrop spectrophotometer (ND-1000, Nanodrop).

Cell experiment:

THP1 cells were cultured using RPMI 1640 with 10 % heat inactivated FBS (fetal bovine serum) and 1 % penicillin / streptomycin. The cells were activated by adding a final concentration of 600ng/mL PMA (phorbol 12-myristate 13-acetate) to 5mL 2*10⁵ cells/mL in 6 well plates and left for 15 min at 37°, 5% CO₂. The media was changed to RPMI 1640 without serum by centrifugation and re-suspension. The cell concentration was adjusted to 1 mil cells/mL and used immediately after activation. Cells were added through a 1mL syringe at 1,8uL/min with a syringe pump. The microchannel and connecting tubing were kept at a constant 37 °C with a Ibidi heated stage. Video recordings were analyzed frame by frame with trackmate, a plugin for the free software FIJI.

Image acquisition:

All fluorescent images were taken on a confocal microscope (LSM700, Zeiss). The microfluidic device was mounted directly on the microscope and images were acquired by imaging inside the buffer filled microchannel. Scanning electron microscopy images were taken on a MagellanTM XHR SEM, FEI. An Olympus IX81 was used for live cell imaging.

Results and discussion:

The microfluidic device setup, including the protein nanopattern is shown in Figure 1. A PDMS slab containing a “Y” shaped microchannel, two inlet, and one outlet (Figure 1a) is irreversibly bonded to a surface with Au nanopatterns spaced by SiO₂ (Figure 1b). We made use of an established colloidal patterning approach^{28, 44} to develop the Au nanopatterns on a cover glass. In brief colloidal nanoparticles were immobilized via electrostatic self-assembly glass samples precoated with Au. The dispersed colloidal particle films were dried and used as a sacrificial mask for physical vapour deposition of a SiO₂ thin film before removal (see figure S1). The spacing parts between the Au nanopatterns were covered by SiO₂ which can be irreversibly bonded to the PDMS slab by a preparatory O₂ plasma treatment step.⁴⁵ The environment exposed to the activated PDMS will change the hydrophobicity and therefore water was added to the microchannel straight after PDMS activation and attachment to the nanopattern⁴⁶. Contact

angle measurements showed that the water drop angle was below detectable limit ($<10^\circ$) for plasma activated PDMS left in water for 24h proving the hydrophilic nature of the PDMS inside the microchannel. The colloidal patterning can be applied over large areas²⁸ and combined with physical vapor deposition to nanopattern entire 5×2.5 cm rectangular glass slides allowing the attachment of several channels per sample, making the microfluidic device a high-throughput platform for the assay. The SiO_2 surface within the channel can be functionalized to provide an anti-fouling surface and/or to further immobilize biomolecules. Here we make use of PLL-g-PEG (poly-L-lysine graft polyethyleneglycol) to render the SiO_2 a robust inert background reducing non-specific protein binding by $>97\%$.²⁸ The remaining parts of the surface (holes through the SiO_2 layer to the underlying Au) provide a second chemistry for functionalization where the diameter of these regions can be defined by the colloidal patterning process in the range 60–3000 nm. The chemical contrast between the SiO_2 and the Au nanopatterns for PLL-g-PEG binding was generated by functionalizing the Au regions via thiol chemistry to prevent the strong attachment of PLL-g-PEG to bare Au and allowing subsequent biomolecule attachment. Sequential attachment of Streptavidin by non-specific and strong attachment was followed by specific binding of biotinylated protein A and subsequent different cell ligands engineered with Fc domains leads to correctly oriented nanoscale domains of cell ligands (Figure 1C). As streptavidin is adsorbed non-specifically it will attach in a random conformation, but as it has four biotin binding sites the exact conformation upon adsorption is not vital. Attachment of biomolecules in the regions between the Au nanopatterns is possible by replacing a fraction of the PLL-g-PEG molecules with NTA (nitrilotriacetic acid)- functionalized PLL-g-PEG allowing the reversible assembly of different HIS-tagged proteins. As illustrated in Figure 1, the protein nanopatterns were assembled inside the channel on to the nanopattern template, simply by adding each reagent (Thiols, PLL-g-PEG and protein solutions) sequentially until the desired pattern was achieved. A scheme outlining the chemical and biological functionalization steps for the full dual protein nanopattern is presented in figure S2. Thiol functionalization of gold is often carried out using alkanethiols which, while making highly stable alkanethiol monolayers, typically requires organic solvents for dissolution.⁴⁷ In this study, however, thiolation processes using organic solvents were unsuccessful in preparing patterns within the microfluidic channels resulting from transfer of thiols into the PDMS material and later re-diffusion out contaminating the substrate of the channel. High quality functionalization was realized using cysteamine which combines the property of being a water soluble thiol and being zwitterionic. Solution based pH selection of a neutral cysteamine during thiolation, to avoid cysteamine binding to the negative SiO_2 layer, and selection of a positive cysteamine charge during PLL-g-PEG functionalization prevents PLL-g-PEG attachment to the gold surface, since the positive charge of the cysteamine layer would electrostatically repel the positively charged lysine in the PLL-g-PEG. The stability of the cysteamine layer is likely low but sufficient to prevent PLL-g-PEG binding to the gold and allow Streptavidin binding. Y-shape channels are known for their ability to form laminar flows where two liquids move down the channel side by side, without mixing. Using this property it is possible to incubate only part of the channel with a specific protein solution, thereby gaining microscale spatial selectivity in the binding process. The nanopatterns were characterized with scanning electron microscopy (SEM) and optical fluorescence microscopy. SEM was performed on samples without protein attachment, and the different-sized nanopatterns obtained by the colloidal lithography process, can be seen directly (Figure 2a). To visualize successfully functionalized protein nanopatterns in the desired way, nanopatterns of fluorescently labelled secondary antibodies (in this case an anti-rabbit antibody labelled with TRITC) were prepared and imaged with fluorescence microscopy (Figure 2b). The pattern of the colloidal lithography generated gold domains is clearly visible in the fluorescence protein patterns with the protein clearly limited to circular domains with well controlled size. To show the

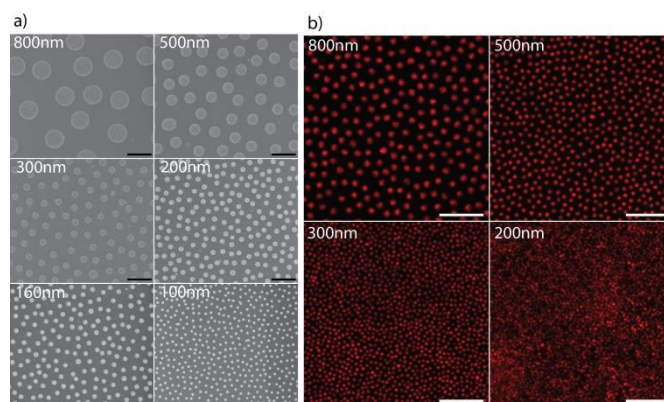


Figure 2: Characterization of the nanopatterns. A) SEM images of the different-sized nanopatterns without protein modification. Au patches with diameters of 800 nm – 100 nm are shown. Scale bar, 1 μm . B) Immunofluorescence staining of protein-A with antibody labelled with TRITC (red) outside microchannels, illustrates the protein nanopatterns for 800 nm – 200 nm patch sizes. Scale bar, 5 μm .

principle of making a dual protein nanopattern, the SiO₂ surface was functionalized with a mixed PLL-g-PEG/PLL-g-PEG-NTA and His-tagged GFP was attached to the PEG-NTA groups. The nanopatterns were modified by protein A, primary antibody to protein A, and TRITC labelled secondary antibody in sequence. To immobilize proteins on the nanopatterns in the whole channel, the proteins were adsorbed to the microchannel sequentially allowing directed deposition onto the substrate inside the whole channel (Figure 3a). To modify the remaining parts of the substrate surrounding the nanopatterns only at the right half of the channel, the his-tagged GFP were infused into the right inlet of the Y-shaped channel and formed laminar flow at the right half of the channel along with the laminar flow at the left half formed by a ringers solution infused via the left inlet with the same flow rate. In Figure 3a, the red fluorescence indicates that the TRITC-labelled secondary antibody was distributed in the entire channel while the green fluorescence indicates that the GFP only immobilized at the right half of the channel. The low (10×) magnification image showed the overall protein distribution within the channel, but cannot resolve the nanopatterns. Higher magnification images (×63 oil immersion) shown in Figure 3b clearly visualized the protein nanopatterns inside the microchannel, 5 representative images (L2, L1, M, R1, R2) were taken across the channel width from the left to the right. The antibody (red) was localized to the nanopattern covering the entire width of the channel. GFP (green) showed the reverse nanopattern, patterning only the regions between the secondary antibody patterns. The merged images, together with the 100× images (Figure 3c), showed how the two nanopatterns aligned perfectly, with minimum background binding in either case. A clear drop can be seen in the intensity of the fluorescence for GFP in the middle image, proving that GFP was accurately confined to one side of the channel. This is also seen from an intensity profile measured on the 10× images, figure S3. Furthermore a low background fluorescence of the channel walls and ceiling was observed, due to PLL-g-PEG attaching to the activated PDMS⁴⁸. As some PLL-g-PEG have NTA tags they will allow binding of HIS-tagged proteins, this could potentially be avoided through the use of other PDMS modification techniques⁴⁹ before PLL-g-PEG is introduced to the channel.

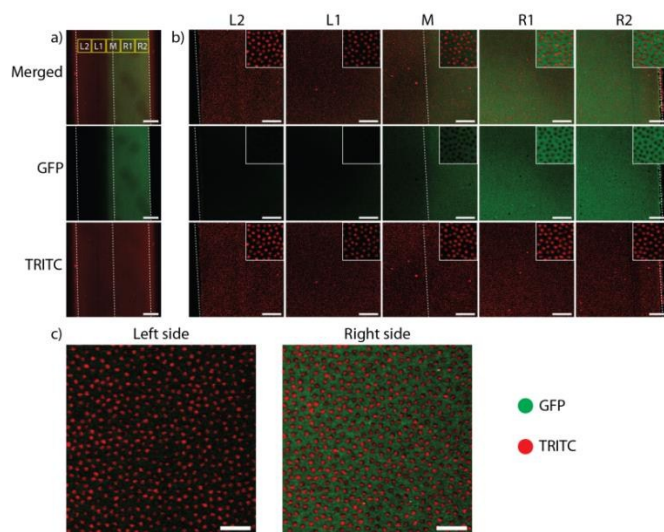


Figure 3: Dual protein nanopattern made inside a microchannel. A GFP his-tagged protein and secondary antibody (TRITC) are used to visualize the two different nanopatterns that can be made. GFP is added under laminar flow conditions limiting its attachment to only one side of the channel. a) A section of the microchannel shows GFP located to one side, while TRITC is attached to the whole channel. The area across the microchannel is divided to 5 regions for imaging at high resolution. From left to right: L2 (left 2), L1 (left 1), M (middle), R1 (right 1), R2 (right 2). 10x magnification, 100µm scale bar. b) Close-up images across the channel shows the two different nanopatterns. GFP forms a reverse nanopattern when compared to TRITC, indicating the high spatial control of the protein attachment. GFP is located only in the right side as seen by the sharp drop in fluorescence in the middle image. 63x magnification, 20µm scale bar. c) High magnification images of both sides of the channel shows the two protein nanopatterns formed. 200x magnification, 5µm scale bar.

We also performed biofunctionalization reverse to those in Figure 3. GFP was incubated in the entire channel, while the TRITC labelled secondary antibody only was allowed to attach to one (right) side. In figure 4, the 10× images show the control over the deposition of the proteins across the channel, with GFP immobilized all across the channel and the antibody confined to the right side (Figure 4a). The GFP reverse nanopattern (Green) has formed throughout the channel, while the secondary antibody nanopatterns (red dots) only visible in one side (Figure 4b). The degree of background binding was minimal as seen in Figure 4c, left side, where the reverse GFP nanopattern is visible, but there was no evidence of any secondary antibody binding to the nanopattern, again illustrating the high spatial control achieved with this method, Figure S3. A relative quantification of the amount of antibody binding was performed and shows the amount of attached antibody depends on the concentration, while also highlighting the reproducibility of the method, figure S4. This could be used to control the density of attached antibody by adjusting the antibody concentration. To achieve a true quantification a method like isotope labeling could be used to precisely determine the amount of protein, but this is out of scope for this paper. A specific biological system where such dual protein

nanopatterns could be applicable would be in the study of leukocyte binding to the endothelium for recruitment to sites of inflammation. These cells are normally freely floating in the blood stream and will under specific circumstances attach to the endothelial cells lining the blood vein and leave the blood circulation. This overall process is well described and is a crucial step in the immune response,¹ and has been shown to be implicated in atherosclerosis⁵⁰. Several cancers are believed to use some of the same mechanisms in metastasis, which, if it occurs, leads to a significantly lower survival chance for the patient.⁴³ Normally binding and exit from circulation is

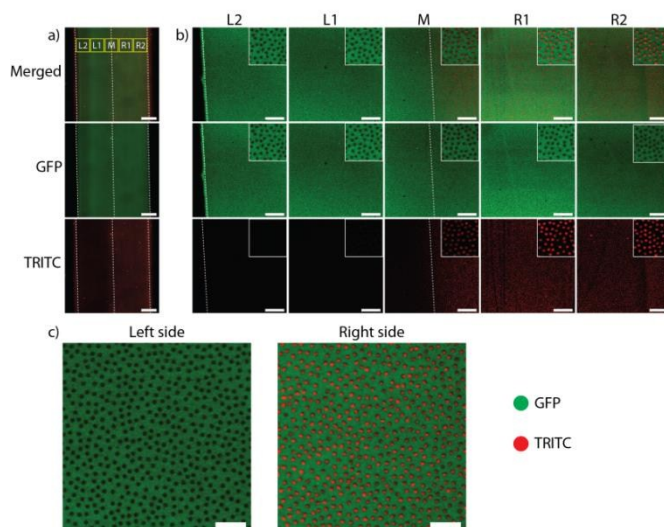


Figure 4: Dual protein nanopattern made inside a microchannel. A GFP his-tagged protein and secondary antibody (TRITC) are used to visualize the two different nanopatterns that can be made. TRITC is added under laminar flow conditions limiting its attachment to only one side of the channel. A) A section of the microchannel shows TRITC located to one side, while GFP is attached to the whole channel. The area across the microchannel is divided to 5 regions for imaging at high resolution. From left to right: L2 (left 2), L1 (left 1), M (middle), R1 (right 1), R2 (right 2). 10x magnification, 100 μ m scale bar. B) Close up images across the channel shows the two different nanopatterns. TRITC is located only in the right side as seen by the sharp drop in fluorescence in the middle image. 63x magnification, 20 μ m scale bar. C) High magnification images of both side of the channel shows the two protein nanopatterns formed. 200x magnification, 5 μ m scale bar.

described as a four step process, namely: rolling adhesion, tight binding, diapedesis and migration. Two separate cell binding ligands are involved in the rolling adhesion and tight binding step which are linked. These two classes of molecules (Selectin's and ICAM's) are believed to show two distinct localizations at the endothelial surface during their interaction with the cell membrane (homogenous and clustered respectively). Here we demonstrate that we can prepare nanostructured microchannels where these two classes of cell binding ligands are co-localized. The rolling of leukocytes is a result of selectins on endothelial cells making weak bonds with sialyl lewis X (SLe^x) regions present on selectin receptors found on leukocytes. The weak nature of the bonds will cause them to repeatedly break and reform, resulting in a rolling behavior. When in close contact with the endothelial cells leukocytes have specific integrins activated allowing the formation of focal adhesions with their ligands, causing the tight binding to the surface. The specific nanoscale distributions of integrin ligands on surfaces has been shown to have a systematic effect on focal adhesion formation in static cell culture.^{26, 28, 31, 51} To show that dual protein nanopatterns can be made of these proteins, three were picked and labelled with fluorophores. For the selectins, P and E selectin were chosen, since they both have been shown to be involved in leukocyte rolling.⁵² ICAM1 was chosen as it is one of the main integrins used in the attachment of leukocytes to the endothelium. ICAM1-FC was allowed to attach to the gold domains of

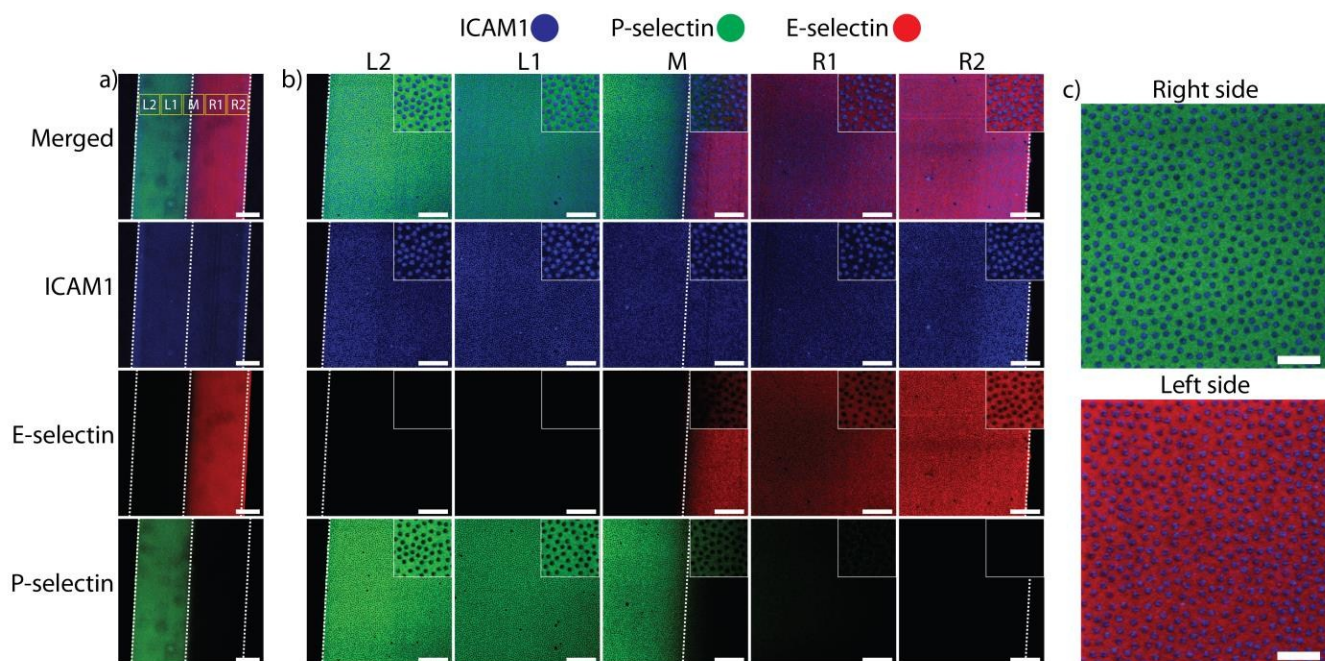


Figure 5: Dual protein nanopattern within a 3-way micropattern made inside a microchannel. ICAM1 (blue), P-selectin (red) and E-selectin (green) have been labelled with specific fluorophores and are visualized inside the microchannel. P- and E- selectin are simultaneously deposited under laminar flow conditions limiting their attachment to opposite sides of the channel. A section of the microchannel showing ICAM1 is found throughout the channel, while P- and E- selectin are confined to one side. The area across the microchannel is divided to 5 regions for imaging at high resolution. From left to right: L2 (left 2), L1 (left 1), M (middle), R1 (right 1), R2 (right 2). 10x magnification, 100 μm scale bar. B) Close up images across the channel shows the two different nanopatterns. The ICAM1 nanopattern is present across the channel, while the reverse nanopattern changes from E-selectin on the left side to P-selectin on the right side. 63x magnification, 20 μm scale bar. C) High magnification images of both side of the channel shows the two distinct protein nanopatterns formed. This illustrates the excellent spatial control of the proteins, both in the microscale and nanoscale range. 200x magnification, 5 μm scale bar.

the whole channel, while P- and E-selectin were added simultaneously, under flow, to opposite sides (P-selectin on the left and E-selectin on the right). By having to selectins localized to either side it would be possible to directly compare any differences in cell behavior. An overview of the channel shows the distribution of the different proteins (Figure 5a). Closer inspection of the channel reveals the ICAM1 nanopattern is formed in the whole channel, while the reverse patterns of P- and E- selectin were located only in the two sides as expected (Figure 5b). There is a clear line down through the channel showing the cut between the two different selectins on the continuous ICAM1 nanopattern. Only trace amounts of either P or E selectins can be found on the opposite sides demonstrating the complete change from one selectin type to the other moving across the channel (Figure S3). The magnified images show the precise distribution between ICAM1 and the selectins (Figure 5c). The ICAM1 nanopattern mimics the focal adhesion formation by presenting pre-clustered ligands for the integrins, and it has been previously shown that by changing the size of the nanopattern dimensions the size of the focal adhesions are also changed, impacting the function of the cell.²⁶ Also the nanopatterning is highly flexible since any HIS-tagged and/or FC-tagged protein/molecule can be used and specifically attached. This multi-protein nanopattern would be ideally suited for studies on leukocyte adhesion and other cells using similar binding methods. To further show the functionality of the nanopattern, the reversible nature of the HIS-tag binding is utilized. The NTA-Histidine binding can be out-competed by adding imidazole, thereby removing any proteins bound to the PEG-NTA groups, without disturbing the FC binding in Au areas. This principle is shown for our system in Figure S5. In Figure S5a GFP is removed and then added to the other side, essentially swapping the overall GFP pattern from one side to the other. Figure S5b shows how it is possible to remove and add GFP to the same side multiple times without getting any rise in the background binding for the other side. Leukocyte binding to a ICAM1 P-selectin channel have been investigated in a proof of principle study to show the effectiveness of this setup. The monocyte-like THP1 cell line was chosen to study their interaction with the nanopattern. ICAM1 nanopatterns were prepared in all parts of the channel and P-selectin reverse nanopatterns were limited to a single side (right side, Figure 6). The cells were activated with PMA to mimic chemokine activation of THP1 integrins. The cells were then exposed to the channel with a flow speed of 1000 $\mu\text{m}/\text{s}$ and a video was recorded to make a live evaluation of the cells interaction with the surface. The majority of the cells were moving very rapidly indicating that they followed the liquid flow without any interaction with the surface. A small proportion of the cells however showed a significantly lower flow speed, and these

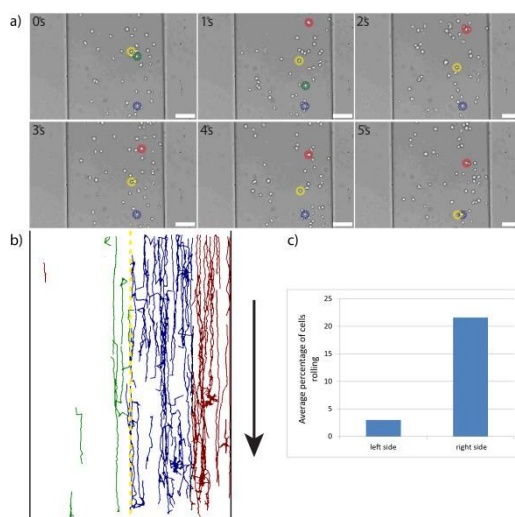


Figure 6: THP1 cells rolling on an ICAM1 nanopattern, where the right side surfaces were modified by reverse P-selectin nanopatterns. a) Single frames, 1 second apart, from a recorded video (11fps). THP1 cells flow by rapidly and cells that interact with the surface are slowed significantly allowing tracking. Colored circles indicate cells interacting with the surface. Each color represents the same cell. Not all interacting cells are shown for clarification. b) Show the cells movement as tracks in part of the channel. Each line represents a single cell rolling on the surface, analyzed from a real time video recording. Only cells in the central part (100 μ m away from the side walls) are used in the data analysis. Red tracks indicate rejected tracks due to their position. Blue tracks are considered to be on the P-selectin side, while green tracks are considered to be on the side with no P-selectin. The Yellow dotted line represents the cut between the left and right side. The channel walls are indicated by black lines. The flow direction is indicated by the arrow. c) Shows the percentage of cells rolling compared to the number of cells that are not interacting with the surface. Only the green and blue tracks shown in b) are used in this analysis. Movie showing the cells flowing in the channel are presented in the electronic supplementary data (Video 1).

were assigned as rolling cells. The tracks of the rolling cells are shown in Figure 6a. From these tracks most features can be extracted, such as rolling velocity, positions, duration and displacement. Here the percentage number of cells rolling compared to the total number of cells was analyzed and shown in Figure 6b. This clearly shows that there is a large increase in cells rolling on the side of P-selectin compared to no P-selectin, which also is evident from looking at Figure 6a. Some cells are completely stopped which could indicate an interaction with ICAM1 to fully arrest the cells on the surface. Imidazole was added after the recording to show the effect of removing P-selectin from the channel. Introducing new cells to the channel showed a very low number of cells rolling on the surface (Figure S6), further validating that the P-selectin is responsible for the slow movement of the cells. The flow rate is important for the cell adhesion and more detailed studies varying the flow rate will be needed to obtain a complete image of the rolling and capture of THP1 cells on the nanopattern presented. By specifically capturing monocytes on a P-selectin / ICAM1 nanopattern this surface is shown to be ideally suited for detailed leukocyte recruitment studies, as it allows direct comparison of protein functions by site specific attachment while having nanoscale control over protein localization. It incorporates both selectin mediated capture and rolling with ICAM1 mediated arrest, the crucial first steps in leukocyte recruitment.

Conclusions:

A new method to incorporate nanopatterns into a microfluidic device has been presented and shown to affect THP1 cells by causing them to roll on the surface in a site specific manner. We make use of PDMS binding to a nanopatterned template and an in-situ all aqueous functionalization process to overcome challenges with microchannel sealing and contamination. We demonstrate a two protein nanopattern applicable to advanced studies on cellular mechanisms under flow. It has previously been shown that a 3-way chemical nanopattern is possible illustrating the potential to expand this method from the dual nanopattern shown in this paper.⁵³ The tunable nanoscale spatial control of multiple proteins, within a microfluidic device, has to the best of our knowledge not been shown before. Being highly flexible in the proteins used, only requiring common tags and straight forward in the method of functionalization it has great potential in several areas. It can easily be integrated into any existing microchannel structure as the nanopattern binds to PDMS, which is the most widely used material for microfluidic structures. It has been shown to affect activated THP1 cells, a monocyte like cell line, causing a rolling behavior and arrest mimicking the first steps in leukocyte binding to an endothelium. This illustrates its potential as a mimic for the initial cell attachment in leukocyte recruitment as the high degree of control over protein localization, both in the mesoscale and nanoscale, protein type and flow should allow advanced and detailed studies not previously possible. Further this method could be used to study cancer metastasis illustrated by the assembly of selectins and integrin ligands in a nanopattern and the effect it has on THP1 behavior. Colloidal lithography

imposes limitations to the possible geometries of nanopatterns, but other more general nanopatterning techniques like E-beam lithography could be used as long as the outermost layer consists of a material that can bind to PDMS. The method presented in this paper can be extended to other research areas since the attachment of proteins is performed with common tags (FC, biotin and His-tags) and the microchannel is made through the commonly used PDMS and the nanopattern is fabricated through a bottom up technique allowing cheap, easy and fast manufacturing.

Acknowledgements:

The work was carried out by funding from the Sino-Danish Center, AUFF travel grant, MOST (2011CB933201, 2012AA030308), CAS (XDA09030305) and NSFC (81361140345, 31470911).

Notes and references

^aInterdisciplinary Nanoscience Center (iNANO), Århus University, Gustav Wiedes vej 14, 8000 Århus, Denmark.

^bNational Center for Nanoscience and Technology (NCNST), 11 ZhongGuanCun BeiYiTiao, Beijing, 100190, China.

Electronic Supplementary Information (ESI) available: Colloidal particle deposition schematic, Intensity profile of fluorescence distributions across channel, reversible nature of HIS-tag binding, and cell tracks after removal of P-selectin is shown in supplementary. Also a video showing cells rolling on the ICAM1/P-selectin nanopattern is available. See DOI: 10.1039/b000000x/

1. K. Ley, C. Laudanna, M. I. Cybulsky and S. Nourshargh, *Nature reviews. Immunology*, 2007, **7**, 678-689.
2. J. Patel, E. McNeill, G. Douglas, A. B. Hale, J. de Bono, R. Lee, A. J. Iqbal, D. Regan-Komito, E. Stylianou, D. R. Greaves and K. M. Channon, *Nat. Commun.*, 2015, **6**.
3. C. Shi and E. G. Pamer, *Nature reviews. Immunology*, 2011, **11**, 762-774.
4. C. Shi, P. Velazquez, T. M. Hohl, I. Leiner, M. L. Dustin and E. G. Pamer, *J Immunol*, 2010, **184**, 6266-6274.
5. B. Leon and C. Ardavin, *Blood*, 2008, **111**, 3126-3130.
6. S. M. Kerfoot and P. Kubers, *The Journal of Immunology*, 2002, **169**, 1000-1006.
7. J. R. Chan, S. J. Hyduk and M. I. Cybulsky, *The Journal of experimental medicine*, 2001, **193**, 1149-1158.
8. G. M. Whitesides, *Nature*, 2006, **442**, 368-373.
9. A. Rival, D. Jary, C. Delattre, Y. Fouillet, G. Castellan, A. Bellemin-Comte and X. Gidrol, *Lab Chip*, 2014, **14**, 3739-3749.
10. T. I. Wong, S. Han, L. Wu, Y. Wang, J. Deng, C. Y. L. Tan, P. Bai, Y. C. Loke, X. D. Yang, M. S. Tse, S. H. Ng and X. Zhou, *Lab Chip*, 2013, **13**, 2405-2413.
11. L. Lin, Y. S. Chu, J. P. Thiery, C. T. Lim and I. Rodriguez, *Lab Chip*, 2013, **13**, 714-721.
12. J. Picot, P. A. Ndour, S. D. Lefevre, W. El Nemer, H. Tawfik, J. Galimand, L. Da Costa, J. A. Ribeil, M. de Montalembert, V. Brousse, B. Le Pioufle, P. Buffet, C. Le Van Kim and O. Francois, *Am. J. Hematol.*, 2015, **90**, 339-345.
13. I. Maschmeyer, A. K. Lorenz, K. Schimek, T. Hasenberg, A. P. Ramme, J. Hubner, M. Lindner, C. Drewell, S. Bauer, A. Thomas, N. S. Sambo, F. Sonntag, R. Lauster and U. Marx, *Lab Chip*, 2015, **15**, 2688-2699.
14. W. Zheng, B. Jiang, D. Wang, W. Zhang, Z. Wang and X. Jiang, *Lab Chip*, 2012, **12**, 3441-3450.
15. Z. Chen, Y. Li, W. Liu, D. Zhang, Y. Zhao, B. Yuan and X. Jiang, *Angewandte Chemie (International ed. in English)*, 2009, **48**, 8303-8305.
16. H. Wu, A. Wheeler and R. N. Zare, *Proc. Natl. Acad. Sci. U. S. A.*, 2004, **101**, 12809-12813.
17. X. Mu, W. Zheng, J. Sun, W. Zhang and X. Jiang, *Small (Weinheim an der Bergstrasse, Germany)*, 2013, **9**, 9-21.
18. X. Jiang, Q. Xu, S. K. W. Dertinger, A. D. Stroock, T.-m. Fu and G. M. Whitesides, *Anal. Chem.*, 2005, **77**, 2338-2347.
19. A. Tourovskaia, X. Figueroa-Masot and A. Folch, *Nat. Protocols*, 2006, **1**, 1092-1104.
20. S. W. Han, S. Lee, J. Hong, E. Jang, T. Lee and W.-G. Koh, *Biosensors and Bioelectronics*, 2013, **45**, 129-135.
21. K. Czondor, M. Garcia, A. Argento, A. Constals, C. Breillat, B. Tessier and O. Thoumine, *Nat. Commun.*, 2013, **4**.
22. R. J. McMurray, N. Gadegaard, P. M. Tsimbouri, K. V. Burgess, L. E. McNamara, R. Tare, K. Murawski, E. Kingham, R. O. C. Oreffo and M. J. Dalby, *Nat Mater*, 2011, **10**, 637-644.
23. M. J. Dalby, N. Gadegaard, R. Tare, A. Andar, M. O. Riehle, P. Herzyk, C. D. W. Wilkinson and R. O. C. Oreffo, *Nature Materials*, 2007, **6**, 997-1003.
24. C. S. Chen, M. Mrksich, S. Huang, G. M. Whitesides and D. E. Ingber, *Science*, 1997, **276**, 1425-1428.
25. B. Trappmann, J. E. Gautrot, J. T. Connelly, D. G. T. Strange, Y. Li, M. L. Oyen, M. A. C. Stuart, H. Boehm, B. J. Li, V. Vogel, J. P. Spatz, F. M. Watt and W. T. S. Huck, *Nature Materials*, 2012, **11**, 642-649.
26. S. H. Kristensen, G. A. Pedersen, L. N. Nejsum and D. S. Sutherland, *Nano Lett.*, 2012, **12**, 2129-2133.
27. S. R. Coyer, A. Singh, D. W. Dumbauld, D. A. Calderwood, S. W. Craig, E. Delamarche and A. J. Garcia, *J Cell Sci*, 2012, **125**, 5110-5123.
28. J. Malmstrom, B. Christensen, H. P. Jakobsen, J. Lovmand, R. Foldbjerg, E. S. Sorensen and D. S. Sutherland, *Nano Lett.*, 2010, **10**, 686-694.
29. M. Arnold, M. Schwieder, J. Blummel, E. A. Cavalcanti-Adam, M. Lopez-Garcia, H. Kessler, B. Geiger and J. P. Spatz, *Soft Matter*, 2009, **5**, 72-77.

30. M. Arnold, E. A. Cavalcanti-Adam, R. Glass, J. Blümmel, W. Eck, M. Kantelehner, H. Kessler and J. P. Spatz, *ChemPhysChem*, 2004, **5**, 383-388.
31. J. E. Gautrot, J. Malmström, M. Sundh, C. Margadant, A. Sonnenberg and D. S. Sutherland, *Nano Lett.*, 2014, **14**, 3945-3952.
32. M. J. Dalby, N. Gadegaard and R. O. C. Oreffo, *Nature Materials*, 2014, **13**, 558-569.
33. R. J. McMurray, N. Gadegaard, P. M. Tsimbouri, K. V. Burgess, L. E. McNamara, R. Tare, K. Murawski, E. Kingham, R. O. C. Oreffo and M. J. Dalby, *Nature Materials*, 2011, **10**, 637-644.
34. J. T. Connelly, J. E. Gautrot, B. Trappmann, D. W. M. Tan, G. Donati, W. T. S. Huck and F. M. Watt, *Nat. Cell Biol.*, 2010, **12**, 711-U177.
35. R. Lutz, K. Pataky, N. Gadhari, M. Marelli, J. Brugger and M. Chiquet, *PLoS ONE*, 2011, **6**, e25459.
36. T. Wolfram, J. Spatz and R. Burgess, *BMC Cell Biology*, 2008, **9**, 64.
37. K. D. Mossman, G. Campi, J. T. Groves and M. L. Dustin, *Science*, 2005, **310**, 1191-1193.
38. M. J. P. Biggs, M. C. Milone, L. C. Santos, A. Gondarenko and S. J. Wind, *Journal of the Royal Society Interface*, 2011, **8**, 1462-1471.
39. M. P. Lutolf, P. M. Gilbert and H. M. Blau, *Nature*, 2009, **462**, 433-441.
40. B. Geiger, J. P. Spatz and A. D. Bershadsky, *Nat Rev Mol Cell Biol*, 2009, **10**, 21-33.
41. J. Herter and A. Zarbock, *Journal of immunology (Baltimore, Md. : 1950)*, 2013, **190**, 4451-4457.
42. R. P. McEver, *Current opinion in cell biology*, 2002, **14**, 581-586.
43. N. Reymond, B. B. d'Agua and A. J. Ridley, *Nat Rev Cancer*, 2013, **13**, 858-870.
44. J. Aizpurua, P. Hanarp, D. S. Sutherland, M. Käll, G. W. Bryant and F. J. García de Abajo, *Physical Review Letters*, 2003, **90**, 057401.
45. D. C. Duffy, J. C. McDonald, O. J. A. Schueller and G. M. Whitesides, *Anal. Chem.*, 1998, **70**, 4974-4984.
46. K. Glasmästar, J. Gold, A.-S. Andersson, D. S. Sutherland and B. Kasemo, *Langmuir*, 2003, **19**, 5475-5483.
47. J. C. Love, L. A. Estroff, J. K. Kriebel, R. G. Nuzzo and G. M. Whitesides, *Chemical reviews*, 2005, **105**, 1103-1169.
48. S. Lee and J. Voros, *Langmuir*, 2005, **21**, 11957-11962.
49. B. Bhushan, D. Hansford and K. K. Lee, *Journal of Vacuum Science & Technology A*, 2006, **24**, 1197-1202.
50. C. Weber and H. Noels, *Nature medicine*, 2011, **17**, 1410-1422.
51. J. Malmstrom, J. Lovmand, S. Kristensen, M. Sundh, M. Duch and D. S. Sutherland, *Nano Lett.*, 2011, **11**, 2264-2271.
52. G. S. Kansas, *Blood*, 1996, **88**, 3259-3287.
53. R. Ogaki, M. A. Cole, D. S. Sutherland and P. Kingshott, *Advanced Materials*, 2011, **23**, 1876-1881.